Carbohydrate Polymers 102 (2014) 653–661

Contents lists available at ScienceDirect

Carbohydrate Polymers

journal homepage: www.elsevier.com/locate/carbpol

Layer-by-layer coated lipid–polymer hybrid nanoparticles designed for use in anticancer drug delivery

Thiruganesh Ramasamy[a], Tuan Hiep Tran[a], Ju Yeon Choi[a], Hyuk Jun Cho[a], Jeong Hwan Kim[a], Chul Soon Yong[a,***], Han-Gon Choi[b,**], Jong Oh Kim[a,*]

[a] College of Pharmacy, Yeungnam University, 214-1, Dae-Dong, Gyongsan 712-749, South Korea
[b] College of Pharmacy, Institute of Pharmaceutical Science and Technology, Hanyang University, 55, Hanyangdaehak-ro, Sangnok-gu, Ansan 426-791, South Korea

ARTICLE INFO

Article history:
Received 28 August 2013
Received in revised form 16 October 2013
Accepted 4 November 2013
Available online 13 November 2013

Keywords:
Layer-by-layer
Polyelectrolyte multilayer
Hybrid solid lipid nanoparticles
Chitosan
Hyaluronic acid
Doxorubicin

ABSTRACT

Polyelectrolyte multilayers created *via* sequential adsorption of complimentary materials may be useful in the delivery of small molecules such as anti-cancer drugs. In this study, layer-by-layer (LbL) nanoarchitectures were prepared by step-wise deposition of naturally derived chitosan and hyaluronic acid on negatively charged hybrid solid lipid nanoparticles (SLNs). A doxorubicin/dextran sulfate complex was incorporated into the SLNs. This resulted in the production of spherical nanoparticles ~265 nm in diameter, with a zeta potential of approximately −12 mV. The nanoparticles were physically stable and exhibited controlled doxorubicin (DOX) release kinetics. Further pharmacokinetic manipulations revealed that in comparison with both free DOX and uncoated DOX-loaded SLNs, LbL-functionalized SLNs remarkably enhanced the circulation half-life and decreased the elimination rate of the drug. Cumulatively, our results suggest that this novel LbL-coated system, with a pH-responsive shell and molecularly targeted entities, has the potential to act as a vehicle to deliver medication to targeted tumor regions.

1. Introduction

Solid lipid nanoparticles (SLNs) have received much attention for their potential to deliver hydrophobic and hydrophilic therapeutic moieties (Kheradmandnia, Vasheghani-Farahani, Nosrati, & Atyabi, 2010; Subedi, Kang, & Choi, 2009; Tran et al., 2013). SLNs are colloidal carriers that combine the advantages of polymeric micelles and lipid-based liposomes (Gohla, & Dingler, 2001; Müller, Mäder, & Gohla, 2000). They have excellent biocompatibility, scalability, and physical stability, and can carry a high drug payload. However, the use of SLNs is associated with burst or premature release *in vivo*, mainly because the particles tend to crystallize and expel the drug from their cores. In addition, SLN-based constructs may be rapidly removed from circulation *via* the activity of the reticulo-endothelial system (RES) (Loomis, Smith, Lee, Yavlovich, & Heldman Blumenthal, 2009). If these nanoparticles are to be used to effectively deliver anti-tumor medication, it will be necessary to overcome these drawbacks by creating a simple, custom-made, release-controlled, surface-modified delivery system.

One new system that shows great potential is polyelectrolyte multilayer (PEM) coatings generated *via* layer-by-layer (LbL) self-assembly of oppositely charged polymers (Boudou, Crouzier, Ren, Blin, & Picart, 2010; Hammond, 2012; Lynn, 2007; Ramasamy & Haidar, 2012). This method of alternative deposition of polyelectrolytes has emerged as a novel approach to functionalize the surface of nanoparticles or to form a core–shell nanoparticle (Jain, Kumar, Swarnakar, & Thanki, 2012; Jiang et al., 2012). PEMs possess the ability to incorporate a broad range of therapeutics in the drug delivery platform. There is mounting evidence that LbL architecture can prolong blood circulation and facilitate enhanced permeation and retention (EPR)-based passive diffusion in interstitial tumors (Becker, Johnston, & Caruso, 2010; Oh et al., 2013). Additionally, the tumor targeting ability of these structures is enhanced by the fact that the layering material is, itself, a targeting moiety (Maeda, Nakamura, Fang, 2012; Poon, Chang, Zhao, & Hammond, 2011). Other key advantages of such core–shell nanoparticles include size, high drug entrapment, controlled drug release, and, perhaps most importantly, a relatively long blood circulation time with tunable *in vivo* functionality (Haidar, Hamdy, & Tabrizian, 2008).

To date, there have been only a handful of studies examining the use of LbL film in loading and targeting tumor regions within

* Corresponding author. Tel.: +82 53 810 2813; fax: +82 53 810 4654.
** Co-corresponding author. Tel.: +82 31 400 5802; fax: +82 31 400 5958.
*** Co-corresponding author. Tel.: +82 53 810 2812; fax: +82 53 810 4654.
E-mail addresses: csyong@yu.ac.kr (C.S. Yong), hangon@hanyang.ac.kr (H.-G. Choi), jongohkim@yu.ac.kr (J.O. Kim).

0144-8617/$ – see front matter © 2013 Elsevier Ltd. All rights reserved.
http://dx.doi.org/10.1016/j.carbpol.2013.11.009

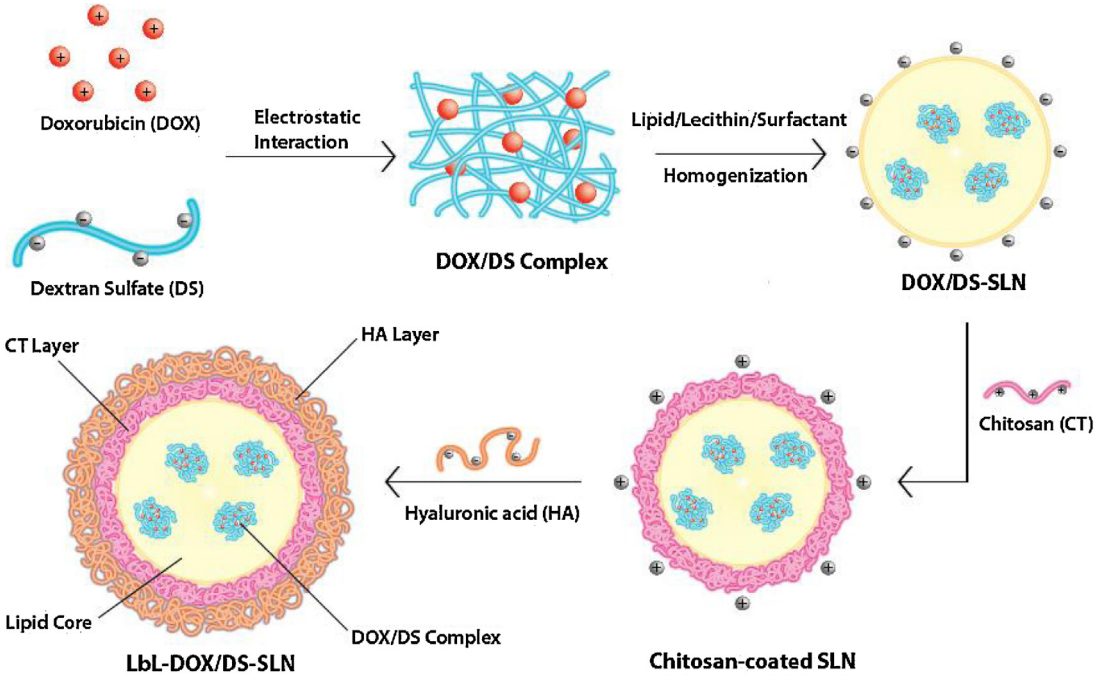

Fig. 1. Diagram illustrating the preparation process for LbL-coated SLNs containing DOX/DS complexes.

the body (Trapani et al., 2011; Yan et al., 2011). Further, none of this previous work investigated whether it is possible to achieve multilayer deposition of charged polymers on drug-loaded and hybrid SLNs. In this study, we used an LbL technique to form a stable core–shell nanoparticle, thus allowing us to combine the advantages of SLNs with those of PEM. We designed three carrier systems: doxorubicin-loaded SLNs (DOX-SLNs), DOX/dextran sulfate complex-loaded SLNs (DOX/DS-SLNs), and LbL-coated DOX/DS-SLNs (LbL-DOX/DS-SLNs). Naturally derived chitosan (CT) and hyaluronic acid (HA) biodegradable polymer pairs, which have excellent biocompatibility and biodegradability, were used as layering materials during construction of the LbL architecture. To explore the suitability of the delivery system, we evaluated physicochemical parameters and performed an *in vitro* release study, a cytotoxicity assay, and several pharmacokinetic experiments.

2. Materials and methods

2.1. Materials

DOX was donated by the Dong-A Pharmaceutical Company (Yongin City, South Korea). Compritol 888 ATO (powder state; melting point, 70 °C) was purchased from Gattefosse (Cedex, France). Soybean lecithin was purchased from Junsei Chemical Co., Ltd. (Tokyo, Japan). Chitosan (low molecular weight; viscosity, 20–200 cps; 85% acetylation), dextran sulfate sodium (MW, 5000 Da), and 3-(4,5-dimethylthiazol-2-yl)-2,5-diphenyl tetrazolium bromide (MTT) reagent were purchased from Sigma–Aldrich (St. Louis, MO, USA). Hyaluronic acid (MW, 3000 Da) was procured from B&K Technology Group Co., Ltd. (Xiamen, China). All other chemicals were of reagent grade and were used as supplied.

2.2. Fabrication of layer-by-layer coated SLNs

SLNs were prepared by the hot homogenization method (Mehnert & Mäder, 2001; Ramasamy, Khandasami, Ruttala, & Shanmugam, 2012). After performing a preliminary analysis of potential lipids and surfactants (data not shown), we decided that Compritol 888 ATO, lecithin, and Tween 80 were best suited for SLN fabrication. Briefly, 300 mg of Compritol 888 ATO and 30 mg of lecithin were melted at 10 °C above the melting point of the lipid to obtain a transparent solution. An aqueous surfactant phase was prepared by dissolving 200 μL of Tween 80 in 10 mL of distilled water, and then heating the solution to the final temperature of the lipid phase. The hot aqueous phase was dispersed in the lipid phase and homogenized (13,500 rpm, 3 min) using an Ultra-Turrax® T-25 homogenizer (IKA-Werke, Staufen, Germany). The resulting coarse emulsion was ultrasonicated (90% amplitude, 3 min) using a probe sonicator (Vibracell VCX130; Sonics, USA). SLNs were obtained by cooling the hot nanoemulsion in an ice bath. DOX-SLNs were prepared by adding 10% w/w of drug to the lipid mixture.

DOX/DS-SLNs were prepared by the same technique with a slight modification. DOX was incubated with DS solutions for 2 h with a mild stirring (200 rpm/min). Both the aqueous surfactant phase and this aqueous phase (heated to 60 °C) were then added to the lipid phase. Otherwise, all other procedures were identical to those described above. DOX/DS complexes were interspersed throughout the SLN core.

To prepare the layer-by-layer DOX/DS-SLNs, we coated anionic charged DOX/DS-SLNs with a cationic CT solution at different volume ratios. The mixture was then incubated for 1 h with a mild shaking, after which an anionic HA solution was added to the positively charged CT-coated SLNs, producing LbL-DOX/DS-SLNs (Fig. 1).

2.3. Measuring hydrodynamic size, ζ-potential, and polydispersity

The dynamic light scattering (DLS) method was used to perform measurements of hydrodynamic size, polydispersity index (PDI), and ζ-potential. Using a Nano-S90 ZetaSizer (Malvern Instruments, Worcestershire, UK), we performed measurements at a fixed scattering angle of 90°. The SLN dispersions were suitably diluted with distilled water (to 50 times less than the original concentration

rendering it ~500 μg/mL) and measured at 25 °C. The hydrodynamic size was determined using the Stokes-Einstein equation. The ζ-potential and PDI were determined using the Nano DTS software (version 6.34) provided by the manufacturer. Each measurement was performed using at least three sets of ten runs.

2.4. Morphological analysis

The morphologies of the different formulations were examined by using a transmission electron microscope (TEM; H7600, Hitachi, Tokyo, Japan) at an accelerating voltage of 100 kV. A drop of the SLN dispersion was placed onto a copper grid coated with a carbon film. After allowing the particles to settle in the grid, negative staining was performed by using phosphotungstic acid (2%, w/v). The copper grid was dried under mild to moderate infrared radiation and then viewed under the microscope.

2.5. Characterization of the physical state

A differential scanning calorimeter (DSC-Q200, TA Instruments, New Castle, DE, USA) was used to study the thermal behavior of the samples. Differential scanning calorimetry (DSC) scans were recorded at a heating rate of 10 °C/min from 40 °C to 250 °C. The experiments were performed in a dynamic nitrogen atmosphere with a flow rate of 50 mL/min. The X-ray diffraction (XRD) patterns of the samples were recorded using a vertical goniometer and X-ray diffractometer (X'Pert PRO MPD diffractometer, Almelo, The Netherlands) to measure Ni-filtered CuKα-radiation (voltage, 40 kV; current, 30 mA) scattered in the crystalline regions of the sample. We employed a scanning rate of 5°/min over the 10–60° diffraction angle (2θ) range at an ambient temperature.

2.6. Drug loading

Drug loading efficiency was determined by ultrafiltration with an Amicon centrifugal filter device (MWCO 10,000 Da, Millipore, Billerica, MA, USA). The drug concentration was determined *via* a standardized colorimetric method. To evaluate the non-encapsulated DOX, we added 2 mL of the SLN dispersion to the ultrafiltration device (10 min at 5000 rpm). After collecting the aqueous filtrate, we determined the final concentration of drug-loaded SLNs by measuring the absorbance at 482 nm with a UV/VIS spectrophotometer (Perkin Elmer U-2800, Hitachi, Tokyo, Japan) (Ramasamy, Kim, Choi, Yong, & Kim, 2014).

2.7. In vitro release study

A dialysis method using membrane tubing (Spectra/Por; 3500 Da cutoff, CA, USA) was used to determine the release profiles of DOX from DOX-SLNs, DOX/DS-SLNs, and LbL-DOX/DS-SLNs. Each construct was placed in phosphate-buffered saline (PBS, pH 7.4, 0.14 M NaCl). The experiment was performed at 37 °C with a shaking speed of 100 rpm. At defined time intervals, whole release medium was replaced with fresh medium to mimic infinite sink conditions. The concentration of DOX present in the dialysate was determined spectrophotometrically by measuring the absorbance at 482 nm. The concentration of the drug released from the SLNs is expressed as a percentage of the total drug available and plotted as a function of time.

2.8. In vitro cytotoxicity assay

The *in vitro* cytotoxicity of free DOX, DOX-SLNs, DOX/DS-SLNs, and LbL-DOX/DS-SLNs was assessed by using the MTT assay, as reported previously (Pradhan et al., 2013). Briefly, 1×10^4 MCF-7 breast cancer cells or A-549 non-small lung cancer cells were seeded in 96-well plates and allowed to attach for 24 h at 37 °C. The cells, which express moderate levels of the CD44 receptor, were exposed to various concentrations of DOX and DOX-SLNs and incubated for 24 h at 37 °C. The cells were washed twice with PBS and maintained in DMEM medium with 10% fetal bovine serum (FBS) for an additional 72 h. After adding 100 μL of MTT (1.25 mg/mL) to each well, we incubated the samples for 3 h at 37 °C in the dark. The cells were then lysed, and the formazan crystals were dissolved in 100 μL of DMSO. Finally, we measured the absorbance at 570 nm by using a microplate reader (Multiskan EX, Thermo Scientific, Waltham, MA, USA); each sample was measured eight times. Cell viability was calculated as $A_{sample}/A_{control} \times 100\%$, where A = absorbance at 570 nm.

2.9. Pharmacokinetic experiments

2.9.1. Study protocols

Male Sprague-Dawley rats weighing 240 ± 10 g were divided into 4 groups of 3 rats. The animals were quarantined in a vivarium maintained at 20 ± 2 °C and 50–60% RH, and fasted for 12 h prior to the experiments. The protocols for the animal studies were approved by the Institutional Animal Ethical Committee, Yeungnam University, South Korea.

2.9.2. Administration and blood collection

The right femoral artery of each rat was cannulated so that blood samples (0.25 mL) could be extracted at designated intervals (0.25, 0.5, 1, 2, 4, 6, 8, 10, 12, and 24 h). The left femoral vein was cannulated to allow administration of free DOX solution, DOX-SLNs, DOX/DS-SLNs, or LbL-DOX/DS-SLNs. The surgical openings were immediately sealed with the help of surgical sutures to ease pain and to increase the length of the study period. After blood was withdrawn, it was immediately centrifuged (Eppendorf, Hauppauge, NY, USA) at 13,000 rpm for 10 min so that plasma could be separated and extracted for further analysis.

2.9.3. Preparation of plasma samples for HPLC

To precipitate proteins out of the plasma samples, 150 μL of plasma was vortex-mixed with 150 μL of acetonitrile for 30 min. The supernatant solution was separated by centrifuging at 13,000 rpm for 10 min, after which the samples were evaporated at 40 °C in a vacuum dryer (Modul 3180C, Buchon, South Korea). The residue was reconstituted in 100 μL of acetonitrile, vortex-mixed, and centrifuged. To quantify drug levels in each plasma sample, 20 μL of the supernatant was injected into the HPLC system, which consisted of a pump (Model L2100), an auto sampler (Model L2200), and an ultraviolet detector (Model L2420; all from Hitachi) used in conjunction with a C_{18} analytic column (Inertsil® ODS3: 0.5 μm, 15 cm × 0.46 cm, GL Sciences Inc., Tokyo, Japan). The mobile phase consisted of methanol:water:acetic acid (50:49:1; pH 2.9) at a flow rate of 1.2 mL/min. The effluent was monitored at a UV absorption wavelength of 280 nm.

2.9.4. Pharmacokinetic data analysis and statistical analysis

A non-compartmental analysis was performed by using WinNonlin software (professional edition, version 2.1; Pharsight Corporation, Mountain View, CA, USA) to calculate the area under the drug concentration–time curve (AUC) from 0 to 24 h, the elimination rate constant (K_{el}), and the half-life ($t_{1/2}$) of the pharmaceuticals. The drug's peak concentration (C_{max}) and time taken to reach the peak concentration (T_{max}) were obtained directly from the plasma *vs.* time profile. ANOVAs were performed to investigate differences between the three experimental treatments. Significance was defined as $p < 0.05$, and all data are expressed as mean ± SD.

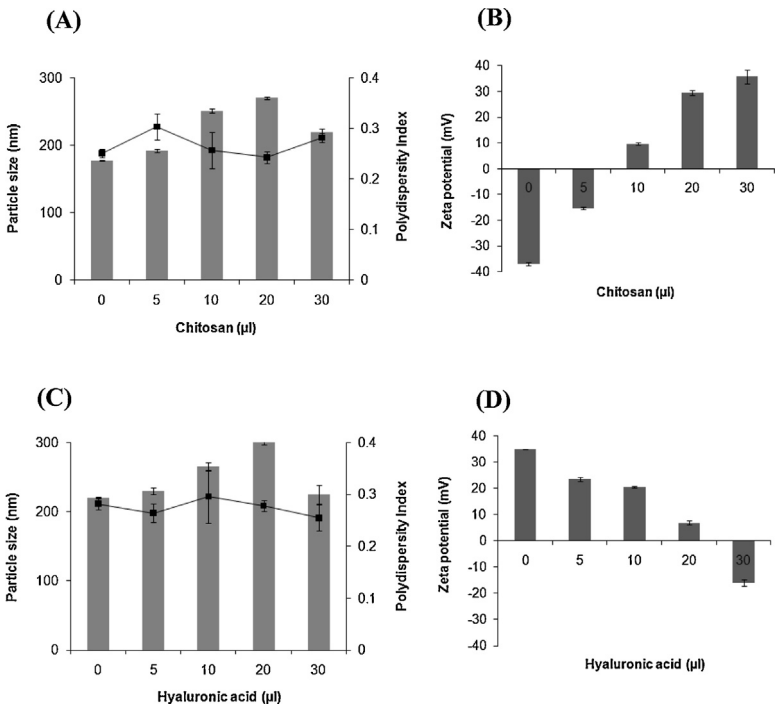

Fig. 2. Characterization of hybrid SLNs during layer-by-layer build-up. Effect of the subsequent deposition of chitosan (CT) and hyaluronic acid (HA) on (A) the hydrodynamic size and polydispersity index, and (B) the corresponding ζ-potential. Concentrations of SLNs, CT, and HA were 1 mg/mL. Initial volume for each sample was 1 mL.

3. Results and discussion

3.1. Fabrication of layer-by-layer hybrid SLNs

Polyelectrolytes were assembled directly on SLNs to prepare a layer-by-layer hybrid SLN. From the vast library of charged polymers, we selected naturally derived CT and HA as cationic and anionic counterparts, respectively. These multifunctional polysaccharides possess excellent biocompatible and anti-fouling properties, the latter of which prevent unnecessary protein adsorption and opsonization in the blood stream (Lee et al., 2008; Morra & Cassineli, 1999; Perrino, Lee, Choi, Maruyama, & Spencer, 2008). In addition, HA is used as a targeting agent in the CD44 over-expressing cancer cell line (Culty, Shizari, Thompson, & Underhill, 1994). Since PEM deposition is primarily governed by electrostatic interactions, the ionic strength, charge density and conformation of weak polyelectrolytes are of prime importance, and are in turn influenced by changes in pH (Alves, Picart, & Mano, 2009). Therefore, we maximized charge density by adjusting the pH of CT ($pK_a = 6.6$) and HA ($pK_a = 4.5$) to 5.5 and 7.0, respectively. In the case of CT, charge density was increased by the protonation of amine groups while for HA, the increase in charge density resulted from ionization of carboxylate groups (Martins, Mano, & Alves, 2010; Ye, Wang, Liu, & Tong, 2005).

The net negative charge present on the surface of the SLNs facilitated alternative deposition of PEM. The SLNs were first prepared by the homogenization method above the melting point of the lipid to obtain a transparent solution. Anionic charged SLNs were then coated with cationic CT solution at different volume ratios. Although hydrodynamic particle size increased with each addition of CT solution during the nanoparticle assembly process, nanoparticle size decreased after the final addition (30 μL; Fig. 2A). Further, the CT addition was associated with a steady shift from approximately −37 mV to +35 mV (Fig. 2B). The minimal change in the zeta potential between the final two additions might have indicated that the surface coating was completed at the higher concentration (Haidar et al., 2008). When the CT was initially added to the negatively charged lipid nanoparticles, electrostatic interactive forces caused a strong interaction to occur. This resulted in the formation of polymer islands on the nanoparticle surface that grew in size with the successive addition of polymer. At this stage, CT neutralized the surface of NP. However, after this neutralization or inflection point, the addition of subsequent polymer created a strong inversion of surface charge, resulting in the formation of a stable and much stiffer NP of a smaller size. The CT blocks on the surface of the NP merged to form a uniform thin layer at the optimal concentration. After this stage, further addition of CT once again increased the size of the NP.

Addition of the second layer (polyanionic HA solution) resulted in particle sizes approaching ~300 nm, though the final size was ~230 nm (Fig. 2C). It is worth noting the approximate 10 nm increase in thickness caused by deposition of the second layer. This pattern is consistent with previous reports that weak polyelectrolytes such as HA undergo exponential growth caused by inter-diffusion of the polymer into the previously adsorbed layer (Picart et al., 2001, 2002). Indeed, CT-HA layer build-up is known to occur on flat surfaces. Further, compared to other polymer pairs that grow linearly as a result of charge overcompensation, HA forms a soft, non-rigid, floppy, and spongy film (Abdelkebir et al., 2011; Hillberg & Tabrizian, 2006; Salomäki & Kankare, 2009). This behavior is also explained by the ability of the shorter HA chains to easily diffuse between the longer CT polymer chains by virtue of strong electrostatic interactions (Calvo, Remunan-lopez, Villa-Jato, & Alonso, 1997). Overall, the bi-layer deposition increased the thickness of the nanoparticle by 50 nm (from ~175 nm prior to deposition to ~225 nm after the final addition).

We also observed good dispersion homogeneity (PDI ~ 0.2) throughout the added layer. The surface charge on the nanoparticle was reversed with the deposition of each alternating polymer, confirming that the film builds in a stepwise fashion driven by alternating electrostatic interactions (Fig. 2D). Thus, our experiments clearly demonstrate that the surface charge on the final LbL-SLNs can be suitably fine-tuned according to our needs. In addition, a final layer of HA can act as both a targeting moiety and a layering

Table 1
Characterization of blank SLN and various DOX-loaded SLN formulations.

	Blank nanoparticles		DOX-loaded nanoparticles		
	SLNs	LbL-SLNs	DOX-SLNs	DOX/DS-SLNs	LbL-DOX/DS-SLNs
Size (nm)	176.4 ± 0.7	225.0 ± 13.4	177.6 ± 2.2	181.7 ± 1.6	264.0 ± 2.2
PDI	0.252 ± 0.008	0.256 ± 0.025	0.302 ± 0.009	0.308 ± 0.016	0.273 ± 0.047
ζ-Potential (mV)	−36.8 ± 0.7	−16.1 ± 1.0	−10.7 ± 0.5	−35.1 ± 0.9	−12.3 ± 2.0
EE[a] (%)	–	–	85.5 ± 2.4	99.5 ± 1.4	97.8 ± 1.3

[a] EE: Entrapment efficiency.

material that controls release kinetics. The success of this technique indicates that it is possible to produce suitably sized LbL nanoparticles with tunable surface charge in order to deliver anticancer drugs at physiological drug barriers *via* the EPR effect. It is also worth noting that our architectural approach to the build-up of core–shell nanoparticles involves a non-washing LbL assembly technique rather than the traditional LbL assembly process based on the sequential precipitation and washing/rinsing of colloidal particles. The exact amount of polyelectrolyte needed to reverse the charge on the drug-loaded nanoparticles in each coating step was carefully evaluated with titration to avoid excess or unnecessary polyelectrolytes.

3.2. Loading of DOX

DOX-SLNs and DOX/DS-SLNs were prepared by adding 10% w/w of the drug to the lipid mixture. Neither DOX-SLNs nor DOX/DS-SLNs showed substantial changes in size after the drug was incorporated into the SLN core. This likely can be attributed to the large size of the core's cavity. However, the addition of the DOX/DS complexes to LbL-DOX/DS-SLNs resulted in a slight increase in size, to approximately 264 nm. This may have resulted from the DS tethering: The CT may interact with both lipids and outward-pointing DS, thereby influencing the architecture build-up and increasing the particle size.

Although the surface charge of the SLNs shifted from -36.9 ± 0.7 to -10.7 ± 0.5 after incorporation of DOX, no such shift was observed in the DOX/DS constructs (Table 1). The shift observed in the DOX-SLNs may reflect partial neutralization of the negatively charged lipid upon encapsulation of the positively charged DOX (Kim, Kabanov, & Bronich, 2009; Kim et al., 2013). On the other hand, the overall lack of change in the DOX/DS-SLNs might have been caused by the anionic DS, which could have completely neutralized the cationic charge on DOX and resulted in only marginal reductions in charge. DS is a naturally derived anionic polysaccharide; its high binding capacity for cationic drugs results from its sulfate moiety. We employed DS to improve drug payload and to tune the release kinetics by overcoming the drug expulsion properties of SLNs.

We achieved an entrapment efficiency (EE) of ~85%, which is much higher than that previously reported (Subedi et al., 2009). The magnitude of the EE may stem from the fact that the large cavity size of our particles could accommodate larger quantities of drugs. In the case of DOX/DS-SLNs, the EE was almost 100% when we employed a 1/0.5 molar ratio for incorporating DOX/DS into the SLNs. The EE of LbL-DOX/DS-SLNs was similarly high, suggesting that the drug was retained either within the core or within the polymer mesh during the LbL assembly process, thus preventing leakage (Table 1).

3.3. Morphological analysis

TEM imaging confirmed the structural morphology of various SLNs in the dried state after the negative staining. TEM imaging of the blank SLNs revealed spherical-shaped nanoparticles with fair particle distribution (Fig. 3A). The CT-coated SLNs possessed PTA-stained SLNs (the dense black spot in the center) surrounded by the CT layer (the lighter stained outer portion; Fig. 3B). It is important

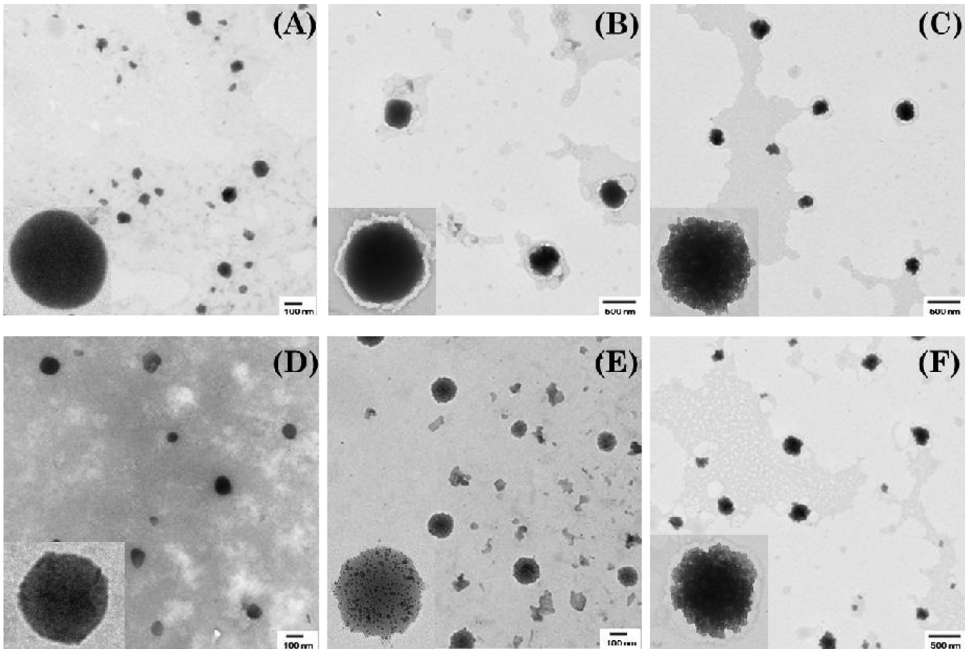

Fig. 3. TEM images of (A) blank SLNs, (B) CT-coated SLNs, (C) LbL-SLNs, (D) DOX-SLNs, (E) DOX/DS-SLNs, and (F) LbL-DOX/DS-SLNs.

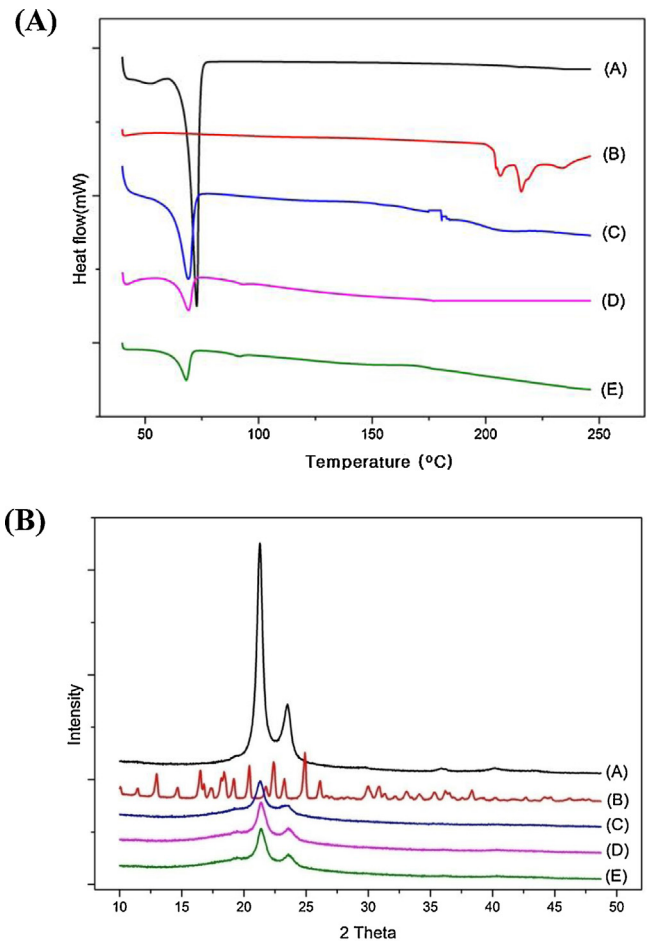

Fig. 4. (A) DSC thermograms and (B) XRD patterns of (a) compritol, (b) free DOX, (c) DOX-SLNs, (d) DOX/DS-SLNs, and (e) LbL-DOX/DS-SLNs.

to note that the polyelectrolyte coating did not alter the spherical shape of the SLNs, and that particle size was consistent with DLS data. Further addition of HA resulted in the formation of a compact core–shell nanoparticle (Fig. 3C). Because of the longitudinal attachment of the polymer chains, we observed no clear distinction between the different polymer layers. Slight conglutination in the polyelectrolyte-coated LbL nanoparticle was due to the irregular stacking of oppositely charged materials on the particle surface. As shown in Fig. 3D, DOX-SLNs retained their spherical shape despite slightly increasing in size after DOX loading. Images of the DOX/DS-SLNs reveal uniform distribution of the DOX-bound DS (indicated by black spots in the SLNs) (Fig. 3E). The darker spots may be caused by a high-electron-density distribution, since the electron density of sulfate (sulfur) is higher than that of other nanoparticle elements. Finally, the TEM imaging of LbL-DOX/DS-SLNs confirmed our previous observation that the particles maintained a spherical shape (Fig. 3F). Overall, the average size of blank SLNs (dried state) was ~100 nm (Fig. 3A) and for LbL-SLNs, it was 200–220 nm with a fairly good dispersity index (Fig. 3C), consistent with the DLS data. In addition, the sizes of DOX-SLNs or DOX/DS-SLNs were ~170 nm (Fig. 3D and E) and LbL-DOX/DS-SLNs were ~250 nm with a slightly broader size distribution (Fig. 3F).

3.4. Physical characterizations

The DSC thermograms of compritol, free DOX, DOX-SLNs, DOX/DS-SLNs, and LbL-DOX/DS-SLNs are shown in Fig. 4A. The DSC measurement is a valuable tool for investigating drug-lipid

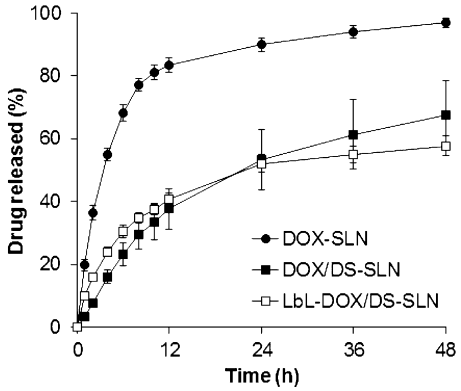

Fig. 5. *In vitro* release profiles of DOX in PBS buffer (pH 7.4, 0.14 M NaCl) at 37 °C. The loading amount of DOX for each sample is 200 μg. Data are expressed as mean ± SD ($n = 3$).

interactions and crystalline behavior. As can be seen, free DOX exhibited a sharp endothermic peak at 220 °C. This corresponds to its melting point and indicates the crystalline nature of the drug. Absence of a comparable endothermic peak from any of the three SLN formulations reveals that the drug was in an amorphous/molecular state after insertion into the particles. This phenomenon is thought to promote drug solubility in the lipid melt and is important for achieving maximum entrapment efficiency (Battaglia et al., 2007; Bunjes, Westesen, & Koch, 1996). Because of the colloidal dimensions of the nanoparticles, as well as their high surface-to-volume ratio, the melting points of lipids in the SLN formulations decreased by ~68 °C (Schubert & Muller-Goymann, 2005).

XRD patterns of compritol, free DOX, DOX-SLNs, DOX/DS-SLNs, and LbL-DOX/DS-SLNs are shown in Fig. 4B. The diffractogram for free DOX showed numerous sharp and intense peaks at several 2θ scattered angles (12.5°, 16.2°, 17.3°, 21.2°, 22.5°, 25.1°, and 26.2°), reflecting its high crystallinity. The lack of a characteristic peak for the SLN formulations indicates complete incorporation of the drug. The peaks at 21° and 24° are associated with lipids. This observation suggests that the drug is either present in its amorphous form or in a molecularly dispersed state within the crystal lattice of the lipid matrices.

3.5. In vitro release study

The release study from SLN formulations was performed in phosphate-buffered saline (pH 7.4) by using a dialysis membrane (Fig. 5). DOX-SLNs exhibited a biphasic release profile, with initial burst release of 50% within 4 h of administration (>80% at 12 h), followed by sustained release over the next 48 h. Use of the DOX/DS-SLN vehicle significantly prolonged the release profile up to 48 h, with only ~35% of the drug released during the first 12 h following administration. This difference in release kinetics between the SLN groups likely stems from the introduction of the DS block to the lipid matrix, within which DOX was electrostatically bound to the DS polymer. The electrostatic interactions between DOX and DS were strong enough to render the complex hydrophobic, thus prolonging its retention in the lipid matrix. Furthermore, the slower release rate observed for DOX/DS-SLNs was probably due to the long path length and the amount of time needed for the drug to detach from the DS block.

The release profile observed for LbL-DOX/DS-SLNs was similar to that recorded for DOX/DS-SLNs (Fig. 5), with ~38% of the drug released during the first 12 h. During the initial period, the DOX release was slightly, albeit noticeably, faster from LbL-DOX/DS-SLNs than from uncoated DOX/DS-SLNs. The major difference between these two particles was evident after 24 h, when the DOX

release from LbL-DOX/DS-SLNs was slower than that from DOX/DS-SLNs.

During LbL assembly of polymers on DOX/DS-SLNs, it is possible that a portion of the drug can extend from the polymer shell, thus facilitating its interaction with the dissolution medium. This could have been responsible for the initial fast release observed from LbL-DOX/DS-SLNs. Once the drug in the outer shell was released, the thickness (density) of the adsorbed PEM would then control release of the drug from the core. The strong ionic interactions between the amine groups of the CT and the carboxyl groups of the HA have the potential to control the degradation of the lipid matrix, thus hindering contact between the drug and the release media. Moreover, the multiple PEM layers increased the diffusional distance, thereby likely causing the tendency for the delayed release we observed during the second half of the study period.

Thus, the LbL coating could potentially facilitate the release of the drug over a longer time scales by preventing initial burst/bolus release from the SLNs. Such drug sequestration has several unique benefits: (a) diminishing the systemic cytotoxicity of the drug, (b) ensuring that the tumor site receives constant, uninterrupted exposure to the drug, and (c) improving the overall therapeutic index of the drug (Ramasamy & Haidar, 2011). Cumulatively, these qualities suggest that LbL-DOX/DS-SLNs could be a very effective new mode of systemic drug delivery.

3.6. Cytotoxicity assay

The cytotoxicity of blank SLN and LbL-SLN was evaluated in MCF-7 breast cancer cells and A-549 non-small lung cancer cells (Fig. 6). Consistent with the excellent biocompatibility of the SLNs and bio-polymers, viability exceeded 80% in MCF-7 cells in the tested concentration range of 0.1–1000 μg/mL (SLNs and LbL-SLNs). In A-549 cells, however, both formulations were slightly toxic (cell viability ~75%) at higher nanoparticle concentrations (1000 μg/mL). This may have been caused by the surfactant. With the exception of this issue, however, SLNs created with Compritol 888 ATO (consisting of mono-, di-, and triglycerides of the long-chained behenic acid) generally exhibited good cytocompatability (Müller, Ruhl, Schulze-Forster, & Mehnert, 1997). The nature and length of this lipid matrix clearly produce a favorable degradation profile, which, in turn, leads to generally low cytotoxicity of blank SLNs (Müller, Ruhl, & Runge, 1996). The low cytotoxicity and high biocompatibility of LbL-SLNs in particular may have been driven by the low molecular weight of both the polymers and the final HA layer. The latter characteristic is likely to have played a prominent role in countering the cytotoxicity previously reported for CT alone; this negative effect may have been prohibited by the negatively charged biocompatible HA terminal layer (Parajó, Angelo, Welle, Fuente, & Alonso, 2010).

We also investigated the dose-dependent cytotoxic effect of DOX-SLN, DOX/DS-SLN, and LbL-DOX/DS-SLN on the viability of MCF-7 and A-549 cell lines (Fig. 7). Maximum cytotoxicity was associated with DOX-SLN treatments, while the lowest was associated with and LbL-DOX/DS-SLNs. Specifically, in comparison to the MCF-7 cell line, the A-549 cell line was more sensitive to the SLN formulations. Although at certain concentrations the SLN formulations applied to MCF-7 cells appeared to cause relatively more cytotoxicity than that observed in drug-free MCF-7 cells, this slight difference was not statistically significant. Therefore, a drug delivery system that could elicit significant cytotoxic actions would provide an invaluable approach for delivery of anticancer drugs, which often encounter stability problems in the blood stream and rapid elimination from a biological system. The high cytotoxic potential of the DOX-SLNs results from the relatively faster release kinetics of DOX-SLNs compared to those of the other two treatments. In sensitive cancer cell lines, free DOX tends to exhibit higher

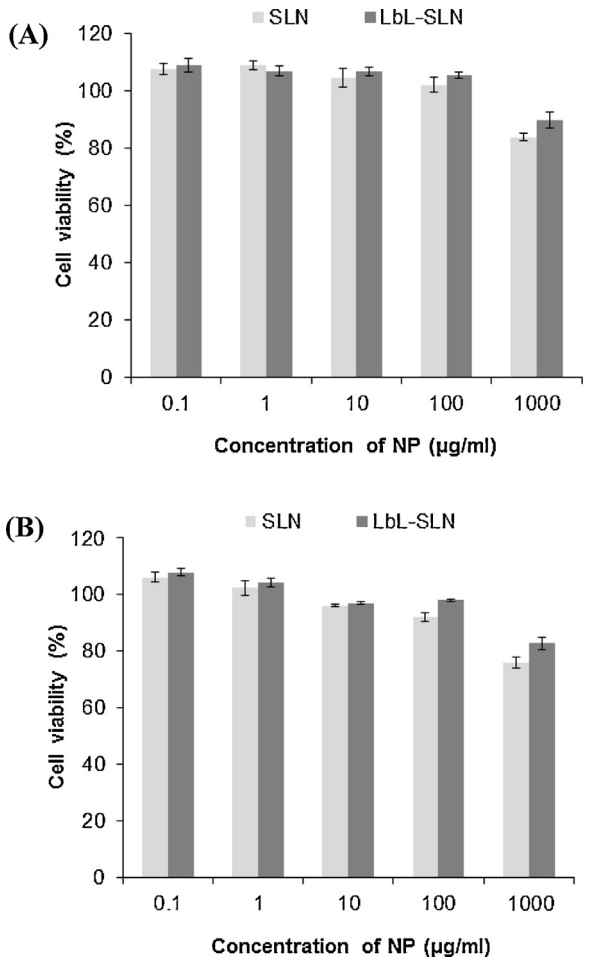

Fig. 6. *In vitro* cytotoxicity of blank SLNs and LbL-SLNs after 24 h of exposure in (A) MCF-7 and (B) A-549 cells. Each value represents the mean ± SD ($n = 8$).

cytotoxicity than that observed for DOX formulations because it is able to penetrate cells *via* passive diffusion (Oh et al., 2013). Our findings, however, suggest that both SLNs and LbL-SLNs increase cell uptake and facilitate sustained intracellular release of the drug. This supports several previous findings that the cytotoxicity of DOX-SLNs is higher than that of free DOX (Fundarò et al., 2000; Subedi et al., 2009; Serpe et al., 2004). Because CD44 acts as the primary cell surface receptor for HA internalization and turnover (Arpicco, Rosa, & Fattal, 2013), we hypothesized that cell uptake of LbL-DOX/DS-SLNs would be high in the two CD44-rich cancer cell lines used here. Surprisingly, we observed the opposite pattern. This may have been caused by the coating system, which could have promoted a sustained and delayed release of the drug.

3.7. Pharmacokinetic study

Fig. 8 shows the plasma concentration–time profiles of DOX following administration of a single intravenous dose (10 mg/kg) of each of the nanoarchitectures into rats. Free DOX was readily cleared from circulation within 6 h of administration (Cho et al., 2012; Gao, Lee, Kim, & Bae, 2005; Ito et al., 2006). In contrast, SLN formulations significantly prolonged circulation of the drug. LbL nanoparticle architecture in particular facilitated maintenance of therapeutic drug levels for the duration of the study period.

We observed significant differences between the SLN formulations and free DOX for several of the pharmacokinetic parameters (Table 2). Specifically, free DOX had higher K_{el}, but lower $t_{1/2}$ and AUC_{all}. Circulation time was notably longer for LbL-DOX/DS-SLNs

Table 2
Pharmacokinetic parameters of DOX after intravenous administration of free DOX, DOX-SLNs, DOX/DS-SLNs, and LbL-DOX/DS-SLNs to rats.

Parameters	Free DOX	DOX-SLNs	DOX/DS-SLNs	LbL-DOX/DS-SLNs
C_{max} (μg/mL)	6.54 ± 1.36	8.71 ± 1.19	9.69 ± 1.38	10.05 ± 1.08
K_{el} (h^{-1})	0.97 ± 0.47	0.13 ± 0.01	0.10 ± 0.01	0.10 ± 0.01
$t_{1/2}$ (h)	0.82 ± 0.32	5.38 ± 0.16	6.80 ± 0.37	7.13 ± 0.34
AUC_{all} (h μg/mL)	7.21 ± 1.14	28.11 ± 3.90	38.72 ± 2.85	44.43 ± 5.98
AUC_{inf} (h μg/mL)	7.22 ± 1.13	30.78 ± 4.3	45.04 ± 4.44	50.70 ± 6.63
MRT	1.64 ± 0.67	8.42 ± 0.34	11.03 ± 0.85	11.05 ± 0.70

Data are expressed as mean ± standard deviation ($n = 3$ per treatment).

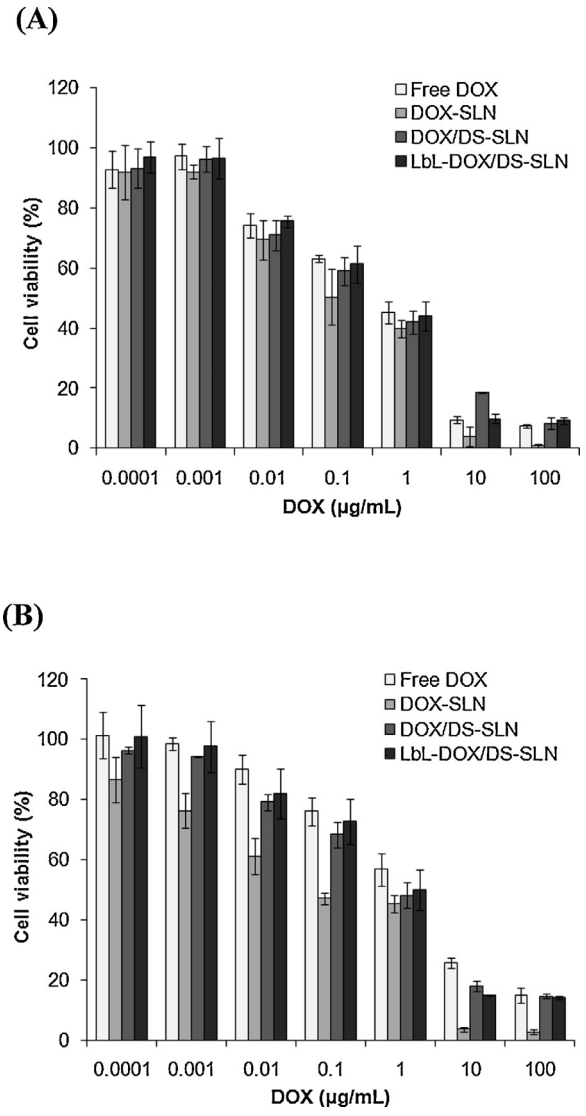

Fig. 7. *In vitro* cytotoxicity of free DOX, DOX-SLNs, DOX/DS-SLNs, and LbL-DOX/DS-SLNs after 24 h of exposure in (A) MCF-7 and (B) A-549 cells. Each value represents the mean ± SD ($n = 8$).

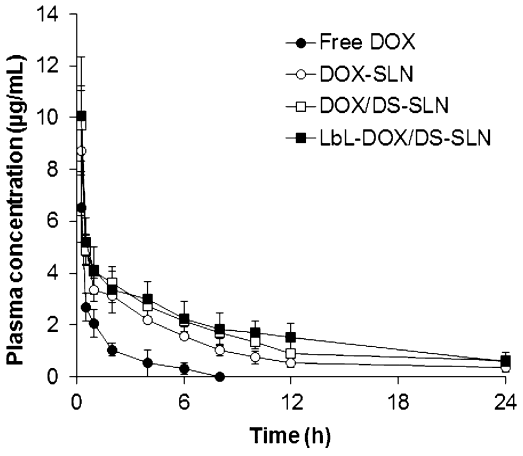

Fig. 8. Plasma concentration–time profiles of free DOX, DOX-SLNs, DOX/DS-SLNs, and LbL-DOX/DS-SLNs administered to rats intravenously. Each value represents the mean ± SD ($n = 3$).

than for either free DOX or the other two nanoarchitectures. The maximum retention time was observed for LbL-DOX/DS-SLNs, with an AUC six times that of the free drug, and 1.5 times that of the DOX-SLNs. These results indicate that the LbL architecture is relatively more stable and has a better pharmacokinetic profile than the other SLN system and support our *in vitro* findings.

The superior performance of LbL architecture can be attributed to several factors. First, the anionic outer layer helps prevent unnecessary interactions between plasma proteins and RES components (Qadi, Meda, Zaghloul, Taboada, & López, 2013). Second, HA itself has anti-fouling properties as a result of the hydrophilic brush-like hydrated coatings that can prolong nanoparticle circulation by minimizing protein adsorption and opsonization. Third, the nanoparticle's small size and protective shell allow the drug to be released in a sustained manner (Lee et al., 2008; Morra & Cassineli, 1999; Perrino et al., 2008). These properties allow LbL-functionalized SLN to remarkably enhance the circulation half-life of the drug, leading to an improved biological performance *in vivo*.

4. Conclusions

The PEM-coated hybrid SLNs were successfully formulated *via* layer-by-layer assembly of CT and HA on DOX/DS-SLNs. The LbL nanoarchitecture build-up was monitored by means of a change in the hydrodynamic size and ζ-potential surface charge. The LbL-DOX/DS-SLNs were relatively stable and exhibited an extended-release phenomenon over a prolonged time period. Our *in vivo* studies indicated that the LbL coating remarkably enhanced the drug and nanoparticle persistence in the blood stream, thus paving the way for efficacious systemic/tumor drug delivery. Nanoparticles exhibited anti-fouling properties as a result of the biomimetic properties of the terminal HA; this, in turn, facilitated an increased circulation half-life and a decreased elimination rate compared to those measured for uncoated SLNs. Cumulatively, our findings not only demonstrate the feasibility of PEM deposition on hybrid SLNs, but also suggest that LbL nanoarchitectures are an exciting and novel therapeutic vehicle for drug delivery.

Acknowledgements

This research was supported by the National Research Foundation of Korea (NRF) grant funded by the Ministry of Education, Science and Technology (no. 2012R1A2A2A02044997 and no. 2012R1A1A1039059).

References

Abdelkebir, K., Gaudière, F., Grognet, S. M., Coquerel, G., Labat, B., Atmani, H., et al. (2011). Evidence of different growth regimes coexisting within biomimetic layer-by-layer films. *Soft Matter*, *7*, 9197–9205.

Alves, N. M., Picart, C., & Mano, J. F. (2009). Self assembling and crosslinking of polyelectrolyte multilayer films of chitosan and alginate studied by QCM and IR spectroscopy. *Macromolecular Bioscience*, *9*, 776–785.

Arpicco, S., Rosa, G. D., & Fattal, E. (2013). Lipid-based nanovectors for targeting of CD44-overexpressing tumor cells. *Journal of Drug Delivery*, *2013* http://dx.doi.org/10.1155/2013/860780 [Article ID 860780], 8 pages

Battaglia, L., Trotta, M., Gallarate, M., Carlotti, M. E., Zara, G. P., & Bargoni, A. (2007). Solid lipid nanoparticles formed by solvent-in-water emulsion–diffusion technique: Development and influence on insulin stability. *Journal of Microencapsulation*, *24*, 672–684.

Becker, A. L., Johnston, A. P. R., & Caruso, F. (2010). Layer-by-layer-assembled capsules and films for therapeutic delivery. *Small*, *6*, 1836–1852.

Boudou, T., Crouzier, T., Ren, K., Blin, G., & Picart, C. (2010). Multiple functionalities of polyelectrolyte multilayer films: New bio-medical applications. *Advanced Materials*, *22*, 441–467.

Bunjes, H., Westesen, K., & Koch, M. H. J. (1996). Crystallization tendency and polymorphic transitions in triglyceride nanoparticles. *International Journal of Pharmaceutics*, *129*, 159–173.

Calvo, P., Remunan-lopez, C., Villa-Jato, J. L., & Alonso, M. L. (1997). Novel hydrophilic chitosanepolyethylene oxide nanoparticles as protein carriers. *Journal of Applied Polymer Sciences*, *63*, 125–132.

Cho, H. J., Yoon, I. S., Yoon, H. Y., Koo, H., Jin, Y. J., Ko, S. H., et al. (2012). Polyethylene glycol-conjugated hyaluronic acid-ceramide self-assembled nanoparticles for targeted delivery of doxorubicin. *Biomaterials*, *33*, 1190–1200.

Culty, M., Shizari, M., Thompson, E. W., & Underhill, C. B. (1994). Binding and degradation of hyaluronan by human breast cancer cell lines expressing different forms of CD44: Correlation with invasive potential. *Journal of Cell Physiology*, *160*, 275–286.

Fundarò, A., Cavalli, R., Bargoni, A., Vighetto, D., Zara, G. P., & Gasco, M. R. (2000). Non-stealth and stealth solid lipid nanoparticles (SLN) carrying doxorubicin: Pharmacokinetics and tissue distribution after i.v. administration to rats. *Pharmacological Research*, *42*, 337–343.

Gao, Z. G., Lee, D. H., Kim, D. I., & Bae, Y. H. (2005). Doxorubicin loaded pH-sensitive micelle targeting acidic extracellular pH of human ovarian A2780 tumor in mice. *Journal of Drug Targeting*, *13*, 391–397.

Gohla, S. H., & Dingler, A. (2001). Scaling up feasibility of the production of solid lipid nanoparticles (SLN™). *Pharmazie*, *56*, 61–63.

Haidar, Z. S., Hamdy, R. C., & Tabrizian, M. (2008). Protein release kinetics for core shell hybrid nanoparticles based on the layer-by-layer assembly of alginate and chitosan on liposomes. *Biomaterials*, *29*, 1207–1215.

Hammond, P. T. (2012). Polyelectrolyte multilayered nanoparticles: using nanolayers for controlled and targeted systemic release. *Nanomedicine*, *7*, 619–622.

Hillberg, A. L., & Tabrizian, M. (2006). Biorecognition through layer-by-layer polyelectrolyte assembly: In-situ hybridization on living cells. *Biomacromolecules*, *7*, 2742–2750.

Ito, T., Tanaka, N. I., Niidome, T., Kawano, T., Kubo, K., Yoshikawa, K., et al. (2006). Hyaluronic acid and its derivative as a multi-functional gene expression enhancer: Protection from non-specific interactions, adhesion to targeted cells, and transcriptional activation. *Journal of Controlled Release*, *112*, 382–388.

Jain, S., Kumar, D., Swarnakar, N. K., & Thanki, K. (2012). Polyelectrolyte stabilized multilayered liposomes for oral delivery of paclitaxel. *Biomaterials*, *33*, 6758–6768.

Jianga, M., Gan, L., Zhu, C., Dong, Y., Liu, J., & Gan, Y. (2012). Cationic core–shell liponanoparticles for ocular gene delivery. *Biomaterials*, *33*, 7621–7630.

Kheradmandnia, S., Vasheghani-Farahani, E., Nosrati, M., & Atyabi, F. (2010). Preparation and characterization of ketoprofen-loaded solid lipid nanoparticles made from beeswax and carnauba wax. *Nanomedicine*, *6*, 753–759.

Kim, J. O., Kabanov, A. V., & Bronich, T. K. (2009). Polymer micelles with cross-linked polyanion core for delivery of a cationic drug doxorubicin. *Journal of Controlled Release*, *138*, 197–204.

Kim, J. O., Ramasamy, T., Yong, C. S., Nukolova, N., Bronich, T. K., & Kabanov, A. V. (2013). Cross-linked polymeric micelles based on block ionomer complexes. *Mendeleev Communications*, *23*, 179–186.

Lee, Y., Lee, H., Kim, Y. B., Kim, J., Hyeon, T., Park, H., et al. (2008). Bioinspired surface immobilization of hyaluronic acid on monodisperse magnetite nanocrystals for targeted cancer imaging. *Advanced Materials*, *20*, 4154–4157.

Loomis, A. P. K., Smith, B., Lee, J. H., Yavlovich, A., & Heldman Blumenthal, R. (2009). Lipid-based nanoparticles as pharmaceutical drug carriers: From concepts to clinic. *Critical Reviews in Therapeutic Drug Carrier System*, *26*, 523–580.

Lynn, D. M. (2007). Peeling back the layers: controlled erosion and triggered disassembly of multilayered polyelectrolyte thin films. *Advanced Materials*, *19*, 4118–4130.

Maeda, H., Nakamura, H., & Fang, J. (2012). The EPR effect for macromolecular drug delivery to solid tumors: Improvement of tumor uptake, lowering of systemic toxicity, and distinct tumor imaging in vivo. *Advanced Drug Delivery Review*, *65*, 71–79.

Martins, G. V., Mano, J. F., & Alves, N. M. (2010). Nanostructured self-assembled films containing chitosan fabricated at neutral pH. *Carbohydrate Polymer*, *80*, 570–573.

Mehnert, W., & Mäder, K. (2001). Solid lipid nanoparticles: Production, characterization and applications. *Advanced Drug Delivery Reviews*, *47*, 165–196.

Morra, M., & Cassineli, C. (1999). Non-fouling properties of polysaccharide-coated surfaces. *Journal of Biomaterials Science: Polymer Edition*, *10*, 1107–1124.

Müller, R. H., Mäder, K., & Gohla, S. (2000). Solid lipid nanoparticles (SLN) for controlled drug delivery – A review of the state of the art. *European Journal of Pharmaceutics and Biopharmaceutics*, *50*, 161–177.

Müller, R. H., Ruhl, D., & Runge, S. A. (1996). Biodegradation of solid lipid nanoparticles as a function of lipase incubation time. *International Journal of Pharmaceutics*, *144*, 115–121.

Müller, R. H., Ruhl, D., Schulze-Forster, K., & Mehnert, W. (1997). Cytotoxicity of solid lipid nanoparticles as a function of the lipid matrix and the surfactant. *Pharmaceutical Research*, *14*, 458–462.

Oh, K. S., Lee, H., Kim, J. Y., Koo, E. J., Lee, E. H., Park, J. H., et al. (2013). The multilayer nanoparticles formed by layer by layer approach for cancer-targeting therapy. *Journal of Controlled Release*, *165*, 9–15.

Parajó, Y., Angelo, I., Welle, A., Fuente, M. G., & Alonso, M. J. (2010). Hyaluronic acid/chitosan nanoparticles as delivery vehicles for VEGF and PDGF-BB. *Drug Delivery*, *17*, 596–604.

Picart, C., Lavalle, P., Hubert, P., Cuisinier, F. J. G., Decher, G., Schaaf, P., et al. (2001). Buildup mechanism for poly(L-lysine)/hyaluronic acid films onto a solid surface. *Langmuir*, *17*, 7414–7424.

Picart, C., Mutterer, J., Richert, L., Luo, Y., Prestwich, G. D., Schaaf, P., et al. (2002). Molecular basis for the explanation of the exponential growth of polyelectrolyte multilayers. *Proceedings of the National Academy of Sciences of the United States of America*, *99*, 12531–12535.

Perrino, C., Lee, S., Choi, S. W., Maruyama, A., & Spencer, N. D. (2008). A biomimetic alter-native to poly(ethylene glycol) as an antifouling coating: Resistance to nonspecific protein adsorption of poly(L-lysine)-graft-dextran. *Langmuir*, *24*, 8850–8856.

Poon, Z., Chang, D., Zhao, X., & Hammond, P. T. (2011). Layer-by-layer nanoparticles with a pH-sheddable layer for in vivo targeting of tumor hypoxia. *ACS Nano*, *5*, 4284–4292.

Pradhan, R., Poudel, B., Ramasamy, T., Choi, H. G., Yong, C. S., & Kim, J. O. (2013). Docetaxel-loaded PLGA nanoparticles: Formulation, physicochemical characterization and cytotoxicity studies. *Journal of Nanoscience and Nanotechnology*, *13*, 5948–5956.

Qadi, S. A., Meda, M. A., Zaghloul, E. M., Taboada, P., & López, C. R. (2013). Chitosan–hyaluronic acid nanoparticles for gene silencing: The role of hyaluronic acid on the nanoparticles' formation and activity. *Colloid and Surface B: Biointerfaces*, *103*, 615–623.

Ramasamy, T., Khandasami, U. S., Ruttala, H., & Shanmugam, S. (2012). Development of solid lipid nanoparticles enriched hydrogels for topical delivery of anti-fungal agent. *Macromolecular Research*, *20*, 682–692.

Ramasamy, T., Kim, J., Choi, H. G., Yong, C. S., & Kim, J. O. (2014). Novel dual drug-loaded block ionomer complex micelles for enhancing the efficacy of chemotherapy treatments. *Journal of Biomedical Nanotechnology* [in press]

Ramasamy, T. G., & Haidar, Z. S. (2011). Characterization and cytocompatibility evaluation of novel core–shell solid lipid nanoparticles for the controlled and tunable delivery of a model protein. *Journal of Bionanoscience*, *5*, 143–154.

Ramasamy, T. G., & Haidar, Z. S. (2012). Alginate-chitosan versus chitosan-alginate multi-layered assembled systems: In situ comparative QCM-D study. *Journal of Biomaterials and Tissue Engineering*, *2*, 83–88.

Salomäki, M., & Kankare, J. (2009). Influence of synthetic polyelectrolytes on the growth and properties of hyaluronan–chitosan multilayers. *Biomacromolecules*, *10*, 294–301.

Schubert, M. A., & Muller-Goymann, C. C. (2005). Characterisation of surface modified solid lipid nanoparticles (SLN): Influence of lecithin and nonionic emulsifier. *European Journal of Pharmaceutics and Biopharmaceutics*, *61*, 77–86.

Serpe, L., Catalano, M. G., Cavalli, R., Ugazio, E., Bosco, O., Canaparo, R., et al. (2004). Cytotoxicity of anticancer drugs incorporated in solid lipid nanoparticles on HT-29 colorectal cancer cell line. *European Journal of Pharmaceutics and Biopharmaceutics*, *58*, 673–680.

Subedi, R. K., Kang, K. W., & Choi, H. K. (2009). Preparation and characterization of solid lipid nanoparticles loaded with doxorubicin. *European Journal of Pharmaceutical Sciences*, *37*, 508–513.

Tran, T. H., Ramasamy, T., Cho, H. J., Kim, Y. I., Poudel, B. K., Choi, H. G., et al. (2013). Formulation and optimization of raloxifene-loaded solid lipid nanoparticles to enhance oral bioavailability. *Journal of Nanoscience and Nanotechnology* [accepted for publication].

Trapani, A., Denora, N., Iacobellis, G., Sitterberg, J., Bakowsky, U., & Kissel, T. (2011). Methotrexate-loaded chitosan- and glycolchitosan-based nanoparticles: A promising strategy for the administration of the anticancer drug to brain tumors. *AAPS PharmSciTech*, *12*, 1302–1312.

Yan, S., Zhu, J., Wang, Z., Yin, J., Zheng, Y., & Chen, X. (2011). Layer-by-layer assembly of poly(L-glutamic acid)/chitosan microcapsules for high loading and sustained release of 5-fluorouracil. *European Journal of Pharmaceutics and Biopharmaceutics*, *78*, 336–345.

Ye, S., Wang, C., Liu, X., & Tong, Z. (2005). Multilayer nanocapsules of polysaccharide chitosan and alginate through layer-by-layer assembly directly on PS nanoparticles for release. *Journal of Biomaterials Science: Polymer Edition*, *16*, 909.